Eur. Phys. J. A **12**, 217–229 (2001)

THE EUROPEAN PHYSICAL JOURNAL A

Isoscalar-isovector interferences in πN $\longrightarrow$ Ne$^+$e$^-$ reactions as a probe of baryon resonance dynamics

A.I. Titov[1,2] and B. Kämpfer[1,a]

[1] Forschungszentrum Rossendorf, PF 510119, 01314 Dresden, Germany
[2] Bogolyubov Laboratory of Theoretical Physics, JINR, Dubna 141980, Russia

Received: 14 August 2001
Communicated by V.V. Anisovich

Abstract. The isoscalar-isovector (ρ-ω) interferences in the exclusive reactions $\pi^- p \to n e^+ e^-$ and $\pi^+ n \to p e^+ e^-$ near the ω threshold leads to a distinct difference of the dielectron invariant-mass distributions depending on beam energy. The strength of this effect is determined by the coupling of resonances to the nucleon vector-meson channels and other resonance properties. Therefore, a combined analysis of these reactions can be used as a tool for determining the baryon resonance dynamics.

PACS. 13.75.-n Hadron-induced low- and intermediate-energy reactions and scattering (energy less than or equal to 10 GeV) – 14.20.-c Baryons (including antiparticles) – 21.45.+v Few-body systems

1 Introduction

The study of dielectron production in hadron and heavy-ion reactions addresses various issues of general interest. In heavy-ion collisions the dileptons are considered as a tool for accessing in-medium modifications of vector mesons. For example, at relativistic energies, the behavior of the ρ-meson attracted much attention because the dilepton data [1] point to a reshuffling of strength in a hot, meson-dominated medium [2,3]. This has been discussed in the wider context of chiral symmetry restoration (cf. [3,4]), QCD sum rules (cf. [5]), and hadronic models (cf. [6]). Likewise, the dielectron production in heavy-ion collisions at beam energies of a $\sim$ 1 AGeV is interesting due to similar reasons. Also here, the dielectron channel is considered as an appropriate tool for studying in-medium modification of vector mesons in a baryon-dense medium. After the first round of experiments with DLS [7], the HADES spectrometer at the heavy-ion synchrotron SIS at GSI/Darmstadt [8], beginning now with experiments, is built to verify these predictions related to fundamental symmetry properties of strong interaction physics. The experimental feasibilities at HADES (*e.g.*, the disposal of beams of pions, protons and a wide range of nuclei) triggered an enhanced activity in this field.

Clearly, for an understanding of dielectron spectra in hadron-nucleus and heavy-ion collisions the elementary hadronic reaction channels must be under control. Here the reactions $NN \to X e^+ e^-$ and $\pi N \to X e^+ e^-$ occupy a highly important place in the dielectron physics. These reactions serve as a necessary input for kinetic approaches (cf. [2,9]). But on the other hand, they are interesting for themselves because they are mainly related to the baryon resonance dynamics. Different facets of the manifestation of baryon resonances in πN collisions have been analyzed in refs. [9–16]. Particularly interesting are such recent theoretical approaches as in [12,14] which attempt a unifying description of meson-nucleon interactions.

The quantum interference in e^+e^- decays of intermediate ρ- and ω-mesons produced in the exclusive reaction $\pi^- p \to n\rho(\omega) \to n e^+ e^-$ has been first discussed in ref. [13], and the first round of HADES experiments will experimentally address this problem [8]. Here, we would like to emphasize that the ρ-ω interference in dielectron production has also an another interesting aspect: The interference may be used as a tool for studying the isoscalar part of the electromagnetic current in the resonance region, what is rather difficult to do by another method. Varying the dilepton invariant-mass M one can test low-lying baryon resonances which are deeply subthreshold for on-shell omega production. Of course, the contribution of the isoscalar part (*i.e.*, the virtual ω production) is much smaller than the dominant isovector (*i.e.*, virtual ρ production) at $M \neq m_\omega$ but it may be clearly seen in the ρ-ω interference which is proportional to the difference of the e^+e^- cross-sections in $\pi^- p$ and $\pi^+ n$ collisions.

Indeed, since the electromagnetic current is the sum of isoscalar and isovector components [17], the invariant amplitude of the reaction $\pi^- p \to n e^+ e^-$ may be expressed as

$$T^{\pi^- p \to n e^+ e^-} \propto T^{\rm scalar} + T^{\rm vector}\,, \qquad (1)$$

[a] e-mail: kaempfer@fz-rossendorf.de

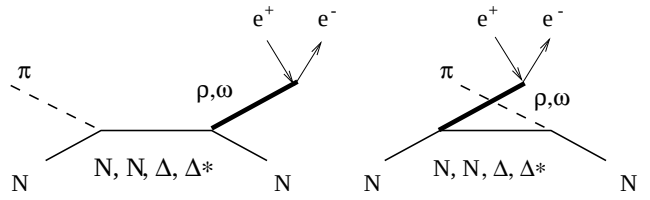

Fig. 1. Diagrammatic representation of the reaction $\pi N \to N e^+ e^-$ for the s and u channels.

where, according to the vector dominance model, the isoscalar (isovector) contributions may be identified with ω- (ρ)-meson intermediate states, *i.e.* $T^{\rm scalar} \propto T^{\omega}$ and $T^{\rm vector} \propto T^{\rho}$. A rotation by 180° around the y-axis in isospin space leads to the transformations $|p\rangle \to -|n\rangle$, $|n\rangle \to |p\rangle$, $|\pi^-\rangle \to -|\pi^+\rangle$, $|\omega\rangle \to |\omega\rangle$, $|\rho^0\rangle \to -|\rho^0\rangle$ and therefore, one gets

$$T^{\pi^+ n \to p e^+ e^-} \propto T^{\rm scalar} - T^{\rm vector}\,. \tag{2}$$

That means, the quantum interferences in the reactions $\pi^- p$ and $\pi^+ n$ are different, and these differences might be well observable in the vicinity of the ω resonance peak.

In ref. [15] the ω production in πN interactions has been analyzed within an approach based on tree level diagrams and effective Lagrangians. A strong contribution in the near-threshold energy region is found to stem from the s and u channels of nucleon and baryon resonances amplitudes. In the present work, we will consider these dominant amplitudes as depicted in fig. 1. (The restriction to s and u channels, and the exclusion of the t channel, is in line with the concept of duality.) We will account for the resonances with mass $M_{B^*} \leq 1.72$ GeV ($B^* = N, N^*, \Delta$). This means that, together with the $T^{\omega} \pm T^{\rho}$ interferences one has to consider the strong "internal" interferences within the ω and ρ channels separately which are in turn different in both channels. Therefore, the proper choice of the $\pi N B^*$, $\omega N N^*$, and $\rho N B^*$ coupling constants and their phases becomes the central problem. To demonstrate the $T^{\omega} \pm T^{\rho}$ interferences within a concise framework we rely mainly on [18], where the relevant coupling constants are expressed in terms of the corresponding couplings to the nucleon by using a quark model. We will also briefly discuss the possibility to use the known partial widths of $B^* \to N\rho$ decays to fix the absolute values of $\rho N B^*$ couplings. Our approach highlights the role of the coupling of subthreshold resonances to the $N\rho$ and $N\omega$ systems (cf. [12,14,19] for discussion and further references).

Our paper is organized as follows. In sect. 2, we define the effective Lagrangians, derive expressions for invariant amplitudes of the processes shown in fig. 1 and discuss the parameter fixing. In sect. 3 the results of numerical calculations and predictions are presented. The summary is given in sect. 4. In the Appendices we show explicit expressions of effective Lagrangians and invariant amplitudes.

2 Amplitudes

The differential cross-section of the reaction $\pi N \to N e^+ e^-$ averaged over the azimuthal angle of the electron is defined as

$$\frac{{\rm d}\sigma}{{\rm d}\Omega {\rm d}\Omega_e {\rm d}M^2} = \frac{\alpha M^2}{8\pi^2}\,\left[\Sigma_{\parallel}\sin^2\Theta + \Sigma_{\perp}(1+\cos^2\Theta)\right], \tag{3}$$

where Ω_e and Θ are the solid and polar angles of the electron, Ω and θ denote the solid and polar angles of the dielectron in the center-of-mass system of the entrance channel, and M stands for the invariant e^+e^- mass. The longitudinal and transversal distributions $\Sigma_{\parallel,\perp}$ read

$$\begin{aligned}
\Sigma_{\parallel} &= \frac{1}{128\pi^2 s}\,\frac{|\mathbf{q}|}{|\mathbf{k}|}\sum_{s_i,s_f}\left|\frac{f_\rho T_\rho^{\lambda=0}{}_{s_i,s_f}}{M^2 - m_\rho^2 + i m_\rho \Gamma_\rho}\right. \\
&\quad \left. + \frac{f_\omega T_\omega^{\lambda=0}{}_{s_i,s_f}}{M^2 - m_\omega^2 + i m_\omega \Gamma_\omega}\right|^2, \\
\Sigma_{\perp} &= \frac{1}{128\pi^2 s}\,\frac{|\mathbf{q}|}{|\mathbf{k}|}\sum_{s_i,s_f}\left|\frac{f_\rho T_\rho^{\lambda=1}{}_{s_i,s_f}}{M^2 - m_\rho^2 + i m_\rho \Gamma_\rho}\right. \\
&\quad \left. + \frac{f_\omega T_\omega^{\lambda=1}{}_{s_i,s_f}}{M^2 - m_\omega^2 + i m_\omega \Gamma_\omega}\right|^2,
\end{aligned} \tag{4}$$

where $k = (E_\pi, \mathbf{k})$ and $q = (E_V, \mathbf{q})$ are the four-momenta of the pion and the dielectron (or the intermediate vector meson) in the center-of-mass system. We denote the four-momenta of the initial (target) and final (recoil) nucleons by p and p'; $s = (p+k)^2$ is the usual Mandelstam variable. $T^{\lambda}_{\rho(\omega)_{s_i,s_f}}$ stands for the invariant amplitude of the virtual vector meson ρ (ω) production with polarization λ and nucleon spin projections s_i, s_f; m_V (with $V = \omega, \rho^0$) is the vector meson mass, f_V denote the coupling constants of the $V \to e^+e^-$ decays, and Γ_V are the total decay widths. For the ω-meson, $\Gamma_\omega = 8.41$ MeV [20], while for the wide ρ-meson, we use the energy-dependent width

$$\Gamma_\rho = \Gamma_\rho{}^0\left[\frac{M^2 - 4m_\pi^2}{m_\rho^2 - 4m_\pi^2},\right]^{\frac{3}{2}}, \tag{5}$$

keeping the strongest M-dependence which comes from the corresponding $\rho\pi\pi$ Lagrangian, with $\Gamma_\rho{}^0 = 150.7$ MeV [20].

The differential invariant-mass distribution integrated over ${\rm d}\Omega_e$ reads

$$\frac{{\rm d}\sigma}{{\rm d}\Omega {\rm d}M^2} = \frac{\alpha M^2}{3\pi}\,\left[\Sigma_{\parallel} + 2\Sigma_{\perp}\right]. \tag{6}$$

2.1 Effective Lagrangians

Calculating the invariant amplitudes for the basic processes shown in fig. 1 we use the following effective interaction Lagrangians in symbolic notation:

$$\mathcal{L}_{\pi N B^*} = f_{\pi N N}\bar\psi_N\,\mathcal{F}_N \boldsymbol{\pi}\cdot\boldsymbol{t}\psi_N + \sum_i f_{\pi N B_i^*}\bar\psi_N\,\mathcal{F}_i \boldsymbol{\pi}\cdot\boldsymbol{t}\psi^i$$

$$+\sum_i f_{\pi N B_i^*}\bar\psi_N\,\mathcal{F}_i^{\alpha}\boldsymbol{\pi}\cdot\boldsymbol{t}\psi^i_{\alpha}$$
$$+\sum_i f_{\pi N B_i^*}\bar\psi_N\,\mathcal{F}_i^{\alpha\beta}\boldsymbol{\pi}\cdot\boldsymbol{t}\psi^i_{\alpha\beta}+\text{h.c.}, \quad (7)$$

$$\mathcal{L}_{\omega NN^*}=g_{\omega NN}\bar\psi_N\,\mathcal{G}^{\mu}_N\psi_N\omega_\mu+\sum_i g_{\omega NN_i^*}\bar\psi_N\,\mathcal{G}_i^{\mu}\psi^i\omega_\mu$$
$$+\sum_i g_{\pi NN_i^*}\bar\psi_N\,\mathcal{G}_i^{\mu\alpha}\psi^i_{\alpha}\omega_\mu$$
$$+\sum_i g_{\pi NN_i^*}\bar\psi_N\,\mathcal{G}_i^{\mu\alpha\beta}\psi^i_{\alpha\beta}\omega_\mu+\text{h.c.}, \quad (8)$$

$$\mathcal{L}_{\rho NB^*}=g_{\rho NN}\bar\psi_N\,\mathcal{G}^{\mu}_N\boldsymbol{\rho}_\mu\cdot\boldsymbol{t}\psi_N+\sum_i g_{\rho NB_i^*}\bar\psi_N\,\mathcal{G}_i^{\mu}\boldsymbol{\rho}_\mu\cdot\boldsymbol{t}\psi^i$$
$$+\sum_i g_{\rho NB_i^*}\bar\psi_N\,\mathcal{G}_i^{\mu\alpha}\boldsymbol{\rho}_\mu\cdot\boldsymbol{t}\psi^i_{\alpha}$$
$$+\sum_i g_{\rho NB_i^*}\bar\psi_N\,\mathcal{G}_i^{\mu\alpha\beta}\boldsymbol{\rho}_\mu\cdot\boldsymbol{t}\psi^i_{\alpha\beta}+\text{h.c.}, \quad (9)$$

where $\boldsymbol{\pi}$, $\boldsymbol{\rho}_\mu$ and ω_μ, are the pion, rho- and omega-meson fields, ψ_N, ψ^i, ψ^i_α and $\psi^i_{\alpha\beta}$ stand for the nucleon, spin-$\frac{1}{2}$, spin-$\frac{3}{2}$ and spin-$\frac{5}{2}$ baryon resonances, respectively. For spin-$\frac{3}{2}$ and $\frac{5}{2}$ fields we use Rarita-Schwinger field operators. $\alpha,\beta,\gamma,\cdots\mu,\nu,\cdots$ are Lorentz indices; i enumerates the corresponding baryon states. The isospin operator $\boldsymbol{t}$ is just Pauli's matrix $\boldsymbol{\tau}$ for the nucleon and nucleon resonances with isospin-$\frac{1}{2}$, while for isospin-$\frac{3}{2}$ it is the transition matrix $\boldsymbol{\chi}$ for delta resonances, see [18]. In the isoscalar amplitude we include the contribution of the nucleon (N) and the 8 resonances (N^*) $P_{11}(1440)$, $D_{13}(1520)$, $S_{11}(1535)$, $S_{11}(1650)$, $D_{15}(1675)$, $F_{15}(1680)$, $D_{13}(1700)$, $P_{13}(1720)$ (the neglect of $P_{11}(1710)$ is motivated in [15]). For the isovector amplitude we consider these states and additionally the 4 Δ states up to 1700 MeV (all together B^*) $P_{33}(1232)$, $P_{33}(1600)$, $S_{31}(1620)$, $D_{33}(1700)$. The explicit form of the employed effective Lagrangians is listed in Appendix A, where the symbols $\mathcal{G}^{\cdots}_{\cdots}$ and $\mathcal{F}^{\cdots}_{\cdots}$ are resolved.

2.2 Invariant amplitudes

The isoscalar invariant amplitude is the coherent sum of nucleon and resonance channels in the following form (the nucleon spin projections are now suppressed):

$$T^\lambda_\omega(N)=g_{\omega NN}\frac{f_{\pi NN}}{m_\pi}\bar u(p')\times\Big[\mathcal{A}_s^{(\omega)\mu}(N)+\mathcal{A}_u^{(\omega)\mu}(N)\Big]u(p)\varepsilon^{*\,\lambda}_\mu\,I_\omega,$$
$$T^\lambda_\omega(N^*)=g_{\omega NN^*}\frac{f_{\pi NN^*}}{m_\pi}\bar u(p')\times\Big[\mathcal{A}_s^{(\omega)\mu}(N^*)+\mathcal{A}_u^{(\omega)\mu}(N^*)\Big]u(p)\varepsilon^{*\,\lambda}_\mu\,I_\omega, \quad (10)$$

where ε^λ_μ is the polarization four-vector for a spin-1 particle with spin projection λ, four-momentum $p=(E,\mathbf{p})$ and mass m

$$\varepsilon^\lambda(p)=\left(\frac{\boldsymbol{\epsilon}^\lambda\cdot\mathbf{p}}{m},\ \boldsymbol{\epsilon}^\lambda+\frac{\mathbf{p}\,(\boldsymbol{\epsilon}^\lambda\cdot\mathbf{p})}{m(E+m)}\right), \quad (11)$$

with the three-dimensional polarization vector $\boldsymbol{\epsilon}$ with components $\boldsymbol{\epsilon}^{\pm1}=\mp\frac{1}{\sqrt2}(1,\pm i,0)$, $\boldsymbol{\epsilon}^0=(0,0,1)$.

The isovector invariant amplitude has a slightly different form because of the corresponding isospin factors

$$T^\lambda_\rho(N)=g_{\rho NN}\frac{f_{\pi NN}}{m_\pi}\bar u(p')\times\Big[\mathcal{A}_s^{(\rho)\mu}(N)-\mathcal{A}_u^{(\rho)\mu}(N)\Big]u(p)\,\varepsilon^{*\,\lambda}_\mu\,I_\rho(N),$$
$$T^\lambda_\rho(N^*)=g_{\rho NN^*}\frac{f_{\pi NN^*}}{m_\pi}\bar u(p')\times\Big[\mathcal{A}_s^{(\rho)^\mu}(N^*)-\mathcal{A}_u^{(\rho)^\mu}(N^*)\Big]u(p)\,\varepsilon^{*\,\lambda}_\mu\,I_\rho(N),$$
$$T^\lambda_\rho(\Delta^*)=g_{\rho N\Delta}\frac{f_{\pi N\Delta}}{m_\pi}\bar u(p')\times\Big[\mathcal{A}_s^{(\rho)^\mu}(\Delta)+\mathcal{A}_u^{(\rho)\mu}(\Delta)\Big]u(p)\,\varepsilon^{*\,\lambda}_\mu\,I_\rho(\Delta), \quad (12)$$

where the isospin factor $I_\rho(N)=-\sqrt2$ for the reaction $\pi^-p\to ne^+e^-$ ($+\sqrt2$ for $\pi^+n\to pe^+e^-$) and $I_\rho(\Delta)=\sqrt2/3$. The s and u channel operators $\mathcal{A}_s^{(\rho,\omega)\mu}$ and $\mathcal{A}_u^{(\rho,\omega)\mu}$ in eq. (10) are defined by the effective Lagrangians of eqs. (7),(8) and listed in Appendix B. $I_\omega=\sqrt2$ is the isospin factor.

Following the previous studies [15,21,22] we assume that the vertices must be dressed by form factors for off-shell baryons

$$F_{B^*}(r^2)=\frac{\Lambda_B^{*4}}{\Lambda_B^{*4}+(r^2-M_{B^*}^2)^2}, \quad (13)$$

where r is the four-momentum of the virtual baryons B^* with mass M_{B^*}. Equation (13) represents the simplest form being symmetric in the s and u channels. The form factor is positive and decreases with increasing off-shellness in both channels.

An analysis of eqs. (10)-(12) shows that i) the interference between s and u channels is different for the ω and ρ production amplitudes, ii) an additional difference comes from the different values and phases of the couplings g_{VNN^*} for the same resonances, and iii) the ρ-ω interference is different for π^-p and π^+n interactions, as already anticipated in eqs. (1),(2).

2.3 Fixing parameters

The coupling constants f_V of the decays $V=\rho,\omega\to e^+e^-$ in eq. (4) are related to the corresponding decay widths as

$$f_V^2=\frac{3\Gamma_{V\to e^+e^-}}{\alpha\,m_V}. \quad (14)$$

Using $\Gamma_{\rho\to e^+e^-}=6.77$ keV and $\Gamma_{\omega\to e^+e^-}=0.60$ keV [20] one gets $f_\rho=0.06$ and $f_\omega=0.0177$. The nucleon and

nucleon resonance amplitudes in fig. 1 are determined by the couplings $f_{\pi NN}$, $f_{\pi NB^*}$, $g_{\omega NN}$, $g_{\omega NN^*}$, $g_{\rho NN}$, $g_{\rho NB^*}$, g_{VNN} and κ_{VNN}, the resonance widths $\Gamma^0_{B^*}$ the branching ratios $B^\pi_{B^*}$, and the cut-offs Λ_B. For the coupling constant $f_{\pi NN}$ we use the standard value $f_{\pi NN} = 1.0$ [18,23]. For the ωNN coupling we use the values $g_{\omega NN} = 10.35$ and $\kappa_{\omega NN} = 0$ determined recently in [18,24]. For the ρNN coupling we use the value $g_{\rho NN} = 3$ and $\kappa_{\rho NN} = 6.1$ [18, 23].

The values of coupling constants $f_{\pi NB^*}$ are determined from a comparison of calculated decay widths $\Gamma_{N^*\to N\pi}$ with the corresponding experimental values [20]. The corresponding signs are taken in accordance with the quark model prediction of ref. [18].

The values of coupling constants g_{VNB^*} follow from $g_{VNB^*} = [g_{VNB^*}/g_{VNN}]g_{VNN}$, where the ratio $[g_{VNB^*}/g_{VNN}]$ is determined by the quark model calculation of ref. [18]. In subsect. 3.2 we contrast this choice of the parameters g_{VNB^*} with another one.

The yet undetermined 13 cut-off parameters Λ_{B^*} in eq. (13) are reduced to one by making the natural assumption

$$\Lambda_N = \Lambda_{B^*} \equiv \Lambda_B. \tag{15}$$

The total cross-section of real ω production in the near-threshold region is reproduced by choosing $\Lambda_B = 0.66$ GeV [15].

3 Results

3.1 Using coupling parameters from [18]

Similar to our previous study of ω production [15] we use the coupling strengths and phases from [18]. For convenience we show in table 1 all the coupling constants, decay widths and branching ratios used in our calculation.

Table 1. Parameters for the resonance masses, coupling constants, total decay widths and branching ratios for $N^* \to N\pi$ decays. The resonance masses and decay widths are in units of MeV.

Baryon	M_{B^*}	$f_{\pi NB^*}$	$g_{\omega NB^*}$	$g_{\rho NB^*}$	$\Gamma^0_{B^*}$	$B^\pi_{B^*}$
$N\frac{1}{2}^+ N$	940	1.0	10.35	3.0	–	–
$N\frac{1}{2}^+ P_{11}$	1440	0.39	6.34	1.78	350	0.65
$N\frac{3}{2}^- D_{13}$	1520	−1.56	8.88	5.0	120	0.55
$N\frac{1}{2}^- S_{11}$	1535	0.36	−5.12	−2.9	150	0.45
$N\frac{1}{2}^- S_{11}$	1650	0.31	2.56	−0.72	150	0.73
$N\frac{5}{2}^- D_{15}$	1675	0.10	10.87	−3.1	150	0.45
$N\frac{5}{2}^+ F_{15}$	1680	−0.42	−14.07	−19.8	130	0.65
$N\frac{3}{2}^- D_{13}$	1700	0.36	2.81	−0.45	100	0.10
$N\frac{3}{2}^+ P_{13}$	1720	−0.25	−3.17	−4.46	150	0.15
$\Delta\frac{3}{2}^+ P_{33}$	1232	2.21	–	17.32	120	0.99
$\Delta\frac{3}{2}^+ P_{33}$	1600	0.52	–	17.1	350	0.18
$\Delta\frac{1}{2}^- S_{31}$	1620	−0.17	–	0.88	150	0.25
$\Delta\frac{3}{2}^- D_{33}$	1700	1.32	–	1.53	300	0.15

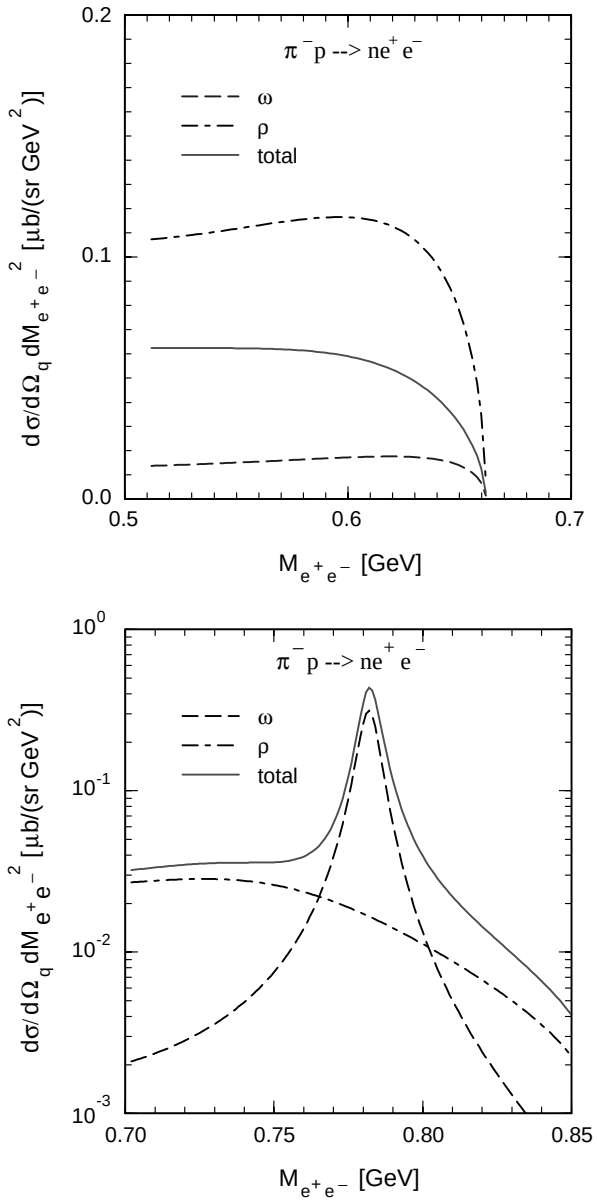

Fig. 2. Differential cross-sections of dielectron production for the reactions $\pi^- p \to n e^+ e^-$ as a function of the dielectron invariant mass for $s^{1/2} = 1.6$ GeV (upper panel) and $s^{1/2} = 1.8$ GeV (lower panel). Dashed and dot-dashed lines correspond to separate ω and ρ contributions, while solid lines are for the coherent sums.

(The masses, decay widths and branching ratios in table 1 represent the averages in [20].) The results of our full calculation of the differential cross-section as a function of dielectron invariant mass are shown in fig. 2 for the reaction $\pi^- p \to n e^+ e^-$ at two energies, $s^{1/2} = 1.6$ and 1.8 GeV. Here and later on, the calculations have been done for the dielectron (or virtual vector meson) production at $\theta = 30^\circ$ in the corresponding center-of-mass system, except for particular cases which are mentioned explicitly below. We also show separately the contributions of the ω and ρ channels. At an energy of $s^{1/2} = 1.8$ GeV

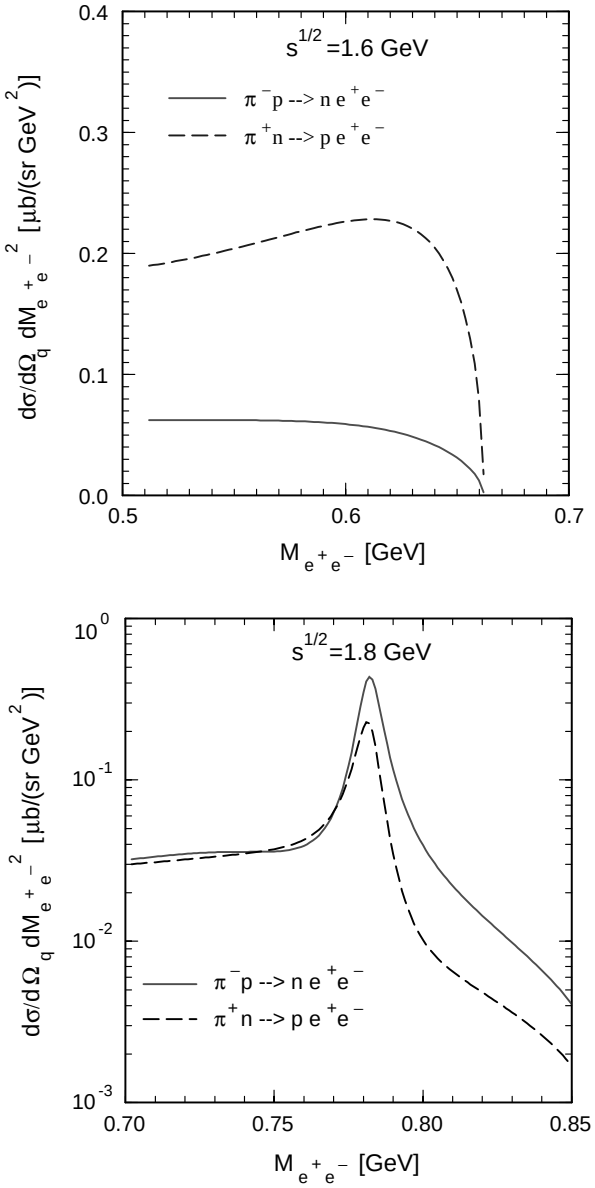

Fig. 3. Differential cross-sections of dielectron production for the reactions $\pi^- p \to n e^+ e^-$ (solid lines) and $\pi^+ n \to p e^+ e^-$ (dashed lines) as a function of dielectron invariant mass for $s^{1/2} = 1.6$ GeV (upper panel) and 1.8 GeV (lower panel).

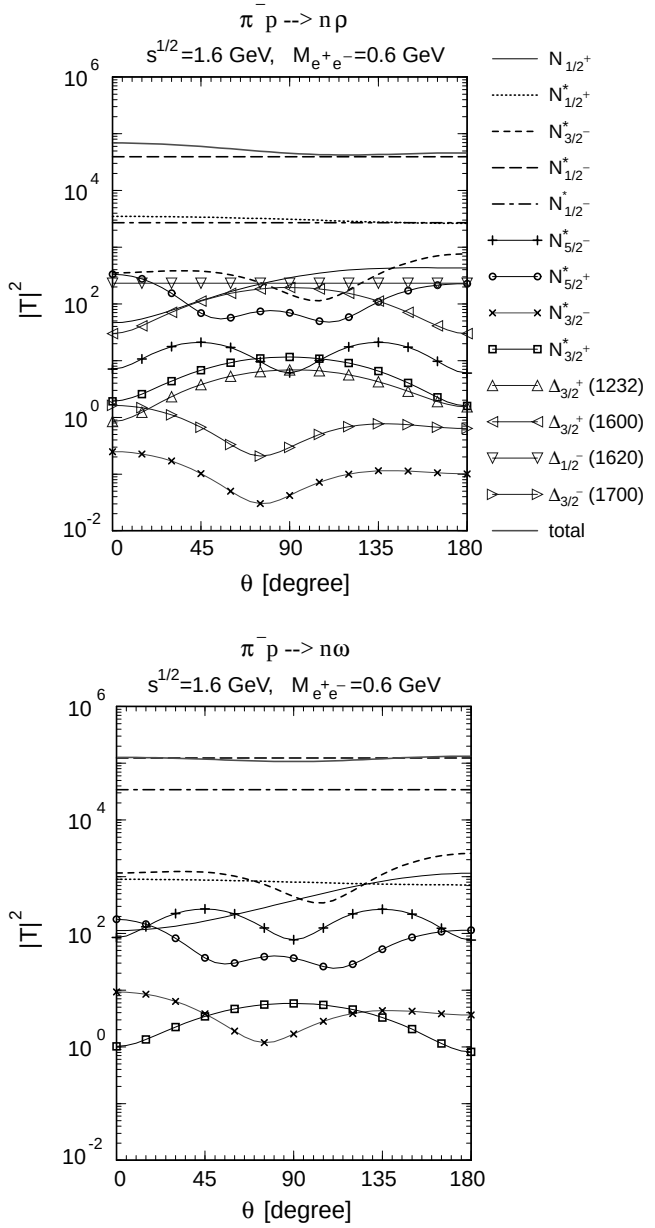

Fig. 4. Angular distribution of the individual contributions of nucleon resonances listed in table 1 to the spin averaged invariant amplitude of ρ (upper panel) and ω (lower panel) channels at $s^{1/2} = 1.6$ GeV and for $M_{e^+e^-} = 0.6$ GeV.

(see fig. 2, lower panel), which is about 80 MeV above the ω production threshold, one can see the sharp ω resonance peak at $M \simeq m_\omega$. Away from the ω peak position one observes a strong decrease of the ω contribution as compared with the fairly flat ρ contribution at the exhibited scale. In contrast, for an energy sufficiently below the ω threshold (fig. 2, upper panel), also the ω contribution is a smooth function of M but below the ρ contribution. This is because the suppression of the resonance factor in eq. (4) at $M \neq m_\omega$ is much stronger for ω.

For the reaction $\pi^+ n \to p e^+ e^-$, the shape of the invariant-mass distribution is similar and therefore, is not displayed here. But the absolute values of the corresponding total distributions are different, and this difference is shown in fig. 3, where the reactions $\pi^- p \to n e^+ e^-$ and $\pi^+ n \to p e^+ e^-$ are compared. The difference reaches a factor up to three and depends on both the energy and the invariant mass. At low energy the cross-section for the reaction $\pi^- p$ is smaller, while at higher energy it is greater than that for $\pi^+ n$ interactions. The reason of this effect is the difference in ρ-ω interferences in the two reactions and a different role of individual baryon resonances depending on the initial energy. In order to get insight into the resonance dynamics, in figs. 4 and 5 we show the contribution of each resonance separately for ρ (upper panels) and ω (lower panels) channels as a function of the di-

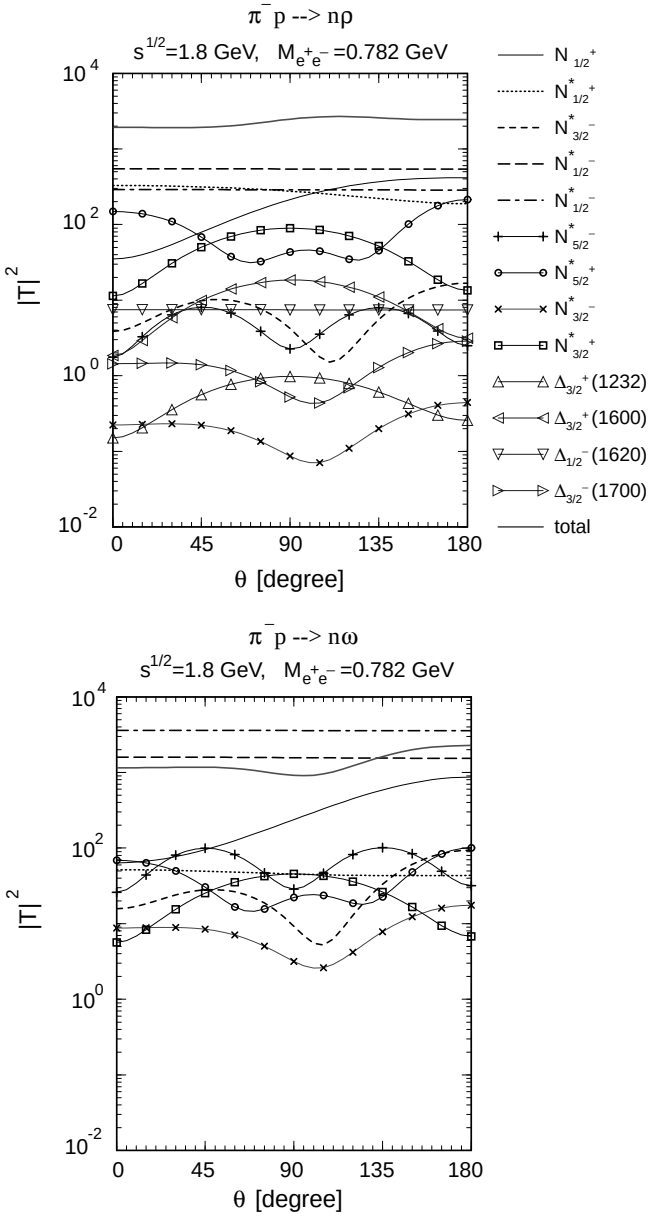

Fig. 5. The same as in fig. 4 but at $s^{1/2} = 1.8$ GeV and $M_{e^+e^-} = 0.782$ GeV.

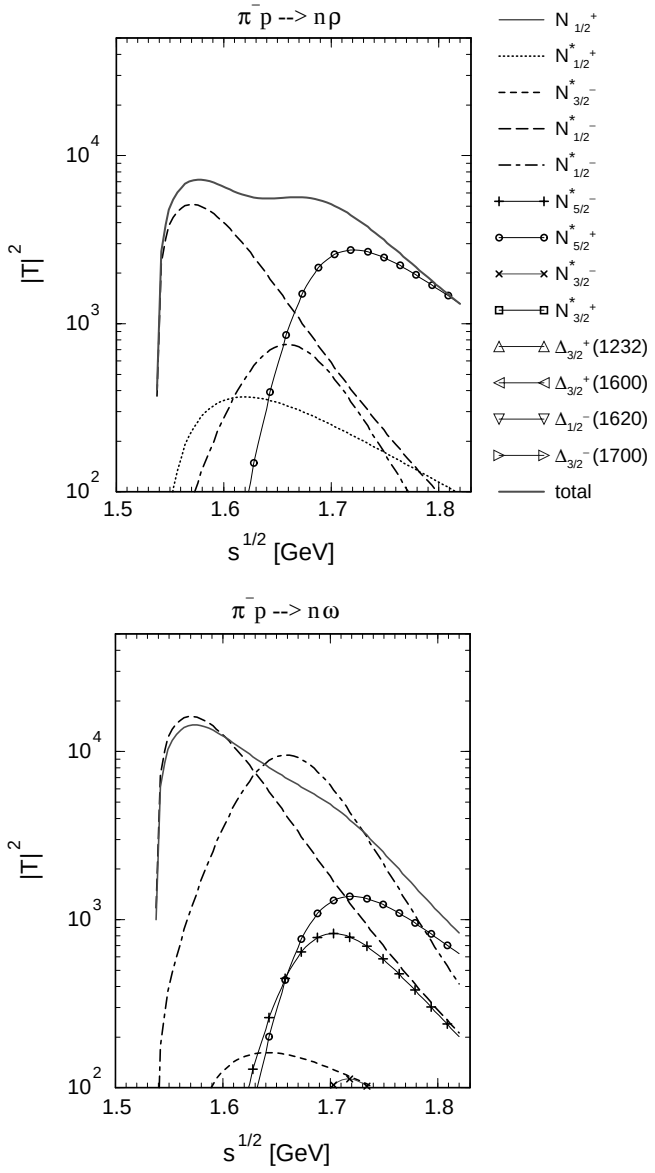

Fig. 6. Individual contributions of nucleon resonances to the spin averaged invariant amplitude of ρ (upper panel) and ω (lower panel) channels as a function of $s^{1/2}$ at $M_{e^+e^-} = 0.6$ GeV.

electron production angle for the reaction $\pi^- p \to n e^+ e^-$. Most transparent is the situation for the ω channel. One can see that dominant contributions come from $S_{11}(1535)$ and $S_{11}(1650)$ resonances. For ω production their phases are opposite, while for ρ production they are the same. At low energy (see fig. 4) the contribution of $S_{11}(1535)$ is greater and taking into account the additional isospin factor I_ρ in eq. (12) we find a destructive total interference at low energy in the reaction $\pi^- p \to n e^+ e^-$, while for $\pi^+ n \to p e^+ e^-$ the interference is constructive. In the ρ channel also the $P_{11}(1440)$ resonance plays a role. At higher energies (see fig. 5) for ω production the $S_{11}(1650)$ resonance is dominant and therefore, the total ρ-ω interference for $\pi^- p \to n e^+ e^-$ ($\pi^+ n \to p e^+ e^-$) becomes constructive (destructive) as depicted in fig. 3. For backward directions, the nucleon channel makes a noticeable contribution.

The relative contribution of different resonances depends on the energy, and this dependence is exhibited in fig. 6 for dominant resonances at $M = 0.6$ GeV. One can see the dominance of $S_{11}(1535)$ at low energy and of $F_{15}(1680)$ at higher energies. The dominance of $S_{11}(1535)$ at low energy leads to a strong destructive (constructive) interference in $\pi^- p \to n e^+ e^-$ ($\pi^+ n \to p e^+ e^-$) reactions shown in fig. 7, where we display the invariant-mass distribution as a function of energy at $M = 0.6$ GeV.

In fig. 8 we show the energy dependence of the invariant-mass distributions at $M = 0.6$ and 0.782 GeV.

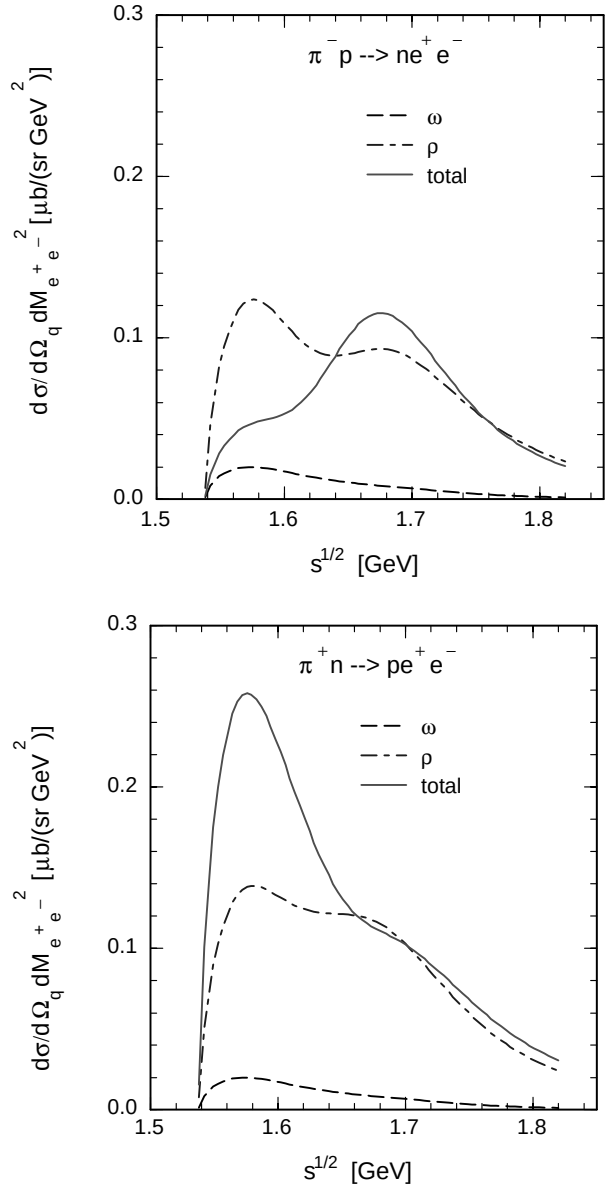

Fig. 7. Differential cross-sections of dielectron production as a function of $s^{1/2}$ for $M_{e^+e^-} = 0.6$ GeV for the reactions $\pi^- p \to ne^+e^-$ (upper panel) and $\pi^+ n \to pe^+e^-$ (lower panel).

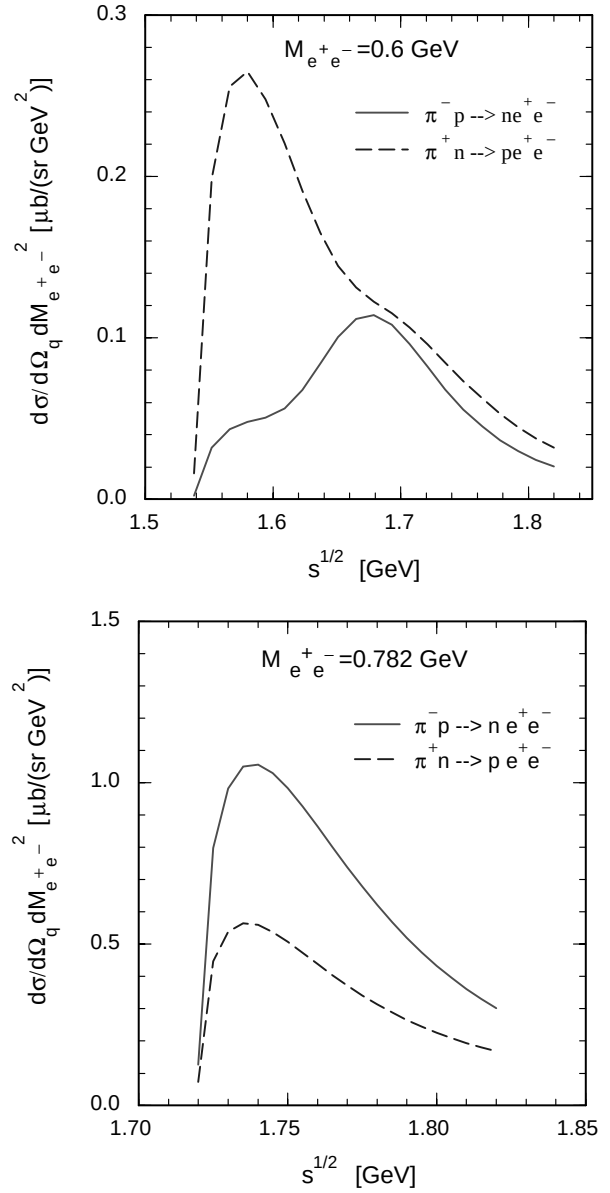

Fig. 8. Differential cross-section of dielectron production for the reactions $\pi^- p \to ne^+e^-$ and $\pi^+ n \to pe^+e^-$ as a function of $s^{1/2}$ for $M_{e^+e^-} = 0.6$ GeV (upper panel) and 0.782 GeV (lower panel).

One can see a striking difference for the two reactions under consideration. There is also a strong sensitivity on changes of the invariant dilepton mass M.

Figure 9 (upper panel) displays the energy dependence of the spin density matrix element ρ_{00}

$$\rho_{00} = \frac{\Sigma_\parallel}{\Sigma_\parallel + 2\Sigma_\perp}, \tag{16}$$

at $\theta = 30°$. One can see a similar qualitative behavior of ρ_{00} for the two reactions. The corresponding angular distributions of electrons, normalized to 1, are shown in fig. 9 (lower panel). We have to note that near threshold ρ_{00} is close to $\frac{1}{3}$ which results in an almost isotropic electron distribution. Far above the threshold, for example at $s^{1/2} = 1.8$ GeV and $M = 0.6$ GeV, the resonance $F_{15}(1680)$ becomes dominant and ρ_{00} exhibits an additional θ-dependence with maxima at $\theta = 0, \pi$ and a minimum at $\theta = \frac{\pi}{2}$, which leads to an anisotropy in the electron decay distributions.

3.2 Adjusting couplings from resonance decays

All the above results are obtained with resonance parameters shown in table 1 and based on the quark model estimates in [18]. In [12,14] coupled-channel calculations are performed with the goal the extract the couplings from a combined analysis of a large set of reaction data. To get an idea on the importance of a particular set of coupling

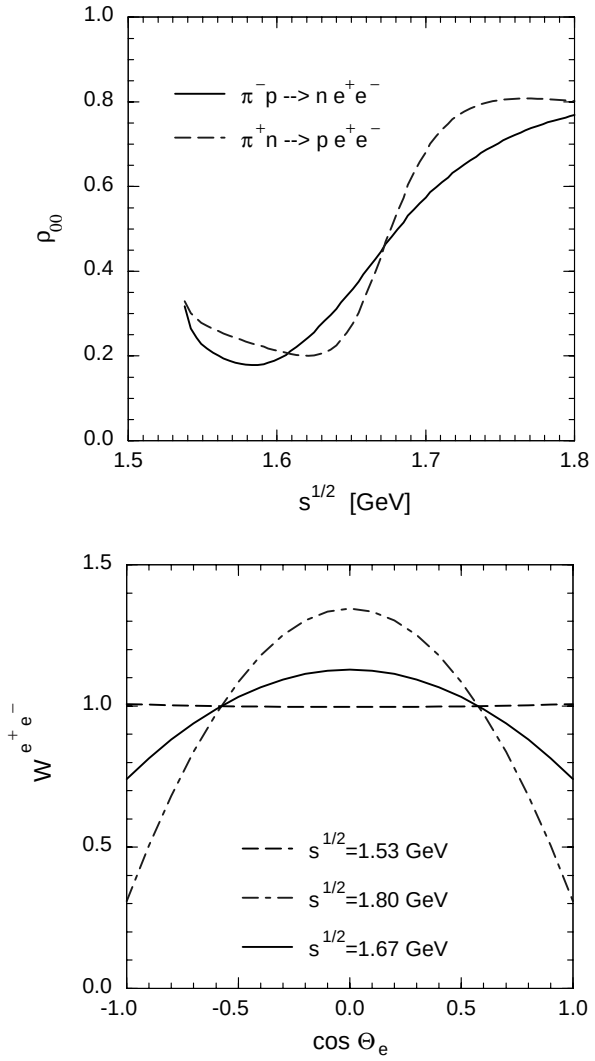

Fig. 9. Spin density matrix element ρ_{00} for $\pi^- p \to n e^+ e^-$ (solid lines) and $\pi^+ n \to p e^+ e^-$ (dashed lines) as a function of $s^{1/2}$ for $M_{e^+e^-} = 0.6$ GeV (upper panel), and the angular distributions of electrons at $M_{e^+e^-} = 0.6$ GeV and different values of $s^{1/2}$ (lower panel).

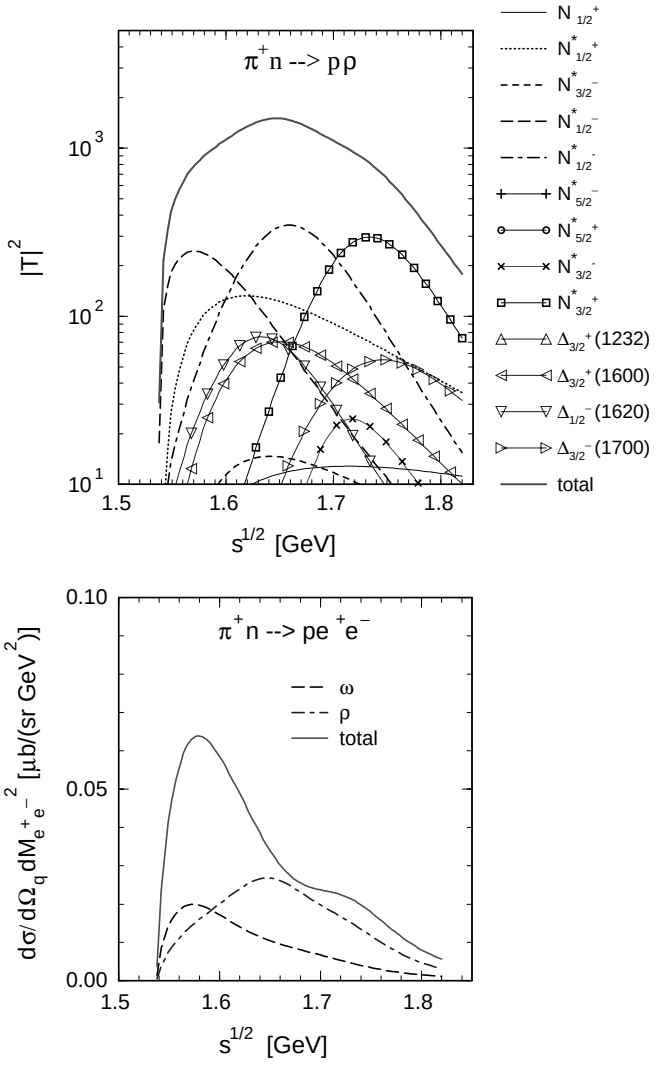

Fig. 10. Upper panel: individual contributions of nucleon resonances listed in table 2 to the spin averaged invariant amplitude of ρ production at $M_{e^+e^-} = 0.6$ GeV. Lower panel: the same as in the lower panel of fig. 7 but with resonance parameters listed in table 2.

strengths within our approach one should compare the above results with such ones which rely on a different set. In principle, one can try to get the absolute values of the $\rho N B^*$ coupling strengths by using the partial branching ratios of the decays $B^* \to N\rho$ [20] via

$$g^{\rm fit}_{\rho N B^*_i}{}^2 = \Gamma_{B^*_i \to N\rho} \left[\frac{2 a_i m_\rho \Gamma_{\rho 0}}{8\pi^2 (2J_i+1) M^2_{B^*_i}} \times \int_{2m_\pi}^{s^{1/2}-M_N} \frac{k(M) F(M) M {\rm d}M}{(M^2 - m_\rho^2)^2 + (m_\rho \Gamma_\rho)^2} \right]^{-1}, \quad (17)$$

where $k(M) = \sqrt{M^2/4 - m_\pi^2}$, $a_i = 3$ (1) for resonances with isospin-$\frac{1}{2}$ ($\frac{3}{2}$), and J_i is the resonance spin. The func-

Table 2. Parameters for the coupling constants $g^{\rm fit}_{\rho N N^*}$ calculated from the partial decay widths $\Gamma_{B^* \to N\rho}$ [20].

Baryon	M_{B^*}	$g^{\rm fit}_{\rho N B^*}$	$B^\rho_{B^*}$
$N\frac{1}{2}^+ P_{11}$	1440	1.07	< 0.08
$N\frac{3}{2}^- D_{13}$	1520	2.70	0.15–0.25
$N\frac{1}{2}^- S_{11}$	1535	-0.63	< 0.04
$N\frac{1}{2}^- S_{11}$	1650	-0.49	0.04–0.12
$N\frac{5}{2}^- D_{15}$	1675	-0.79	0.01–0.03
$N\frac{5}{2}^+ F_{15}$	1680	-1.19	0.03–0.15
$N\frac{3}{2}^- D_{13}$	1700	-1.31	< 0.35
$N\frac{3}{2}^+ P_{13}$	1720	-13.9	0.7–0.85
$\Delta\frac{3}{2}^+ P_{33}$	1600	41.0	< 0.25
$\Delta\frac{1}{2}^- S_{31}$	1620	1.39	0.07–0.25
$\Delta\frac{3}{2}^- D_{33}$	1700	4.27	0.30–0.55

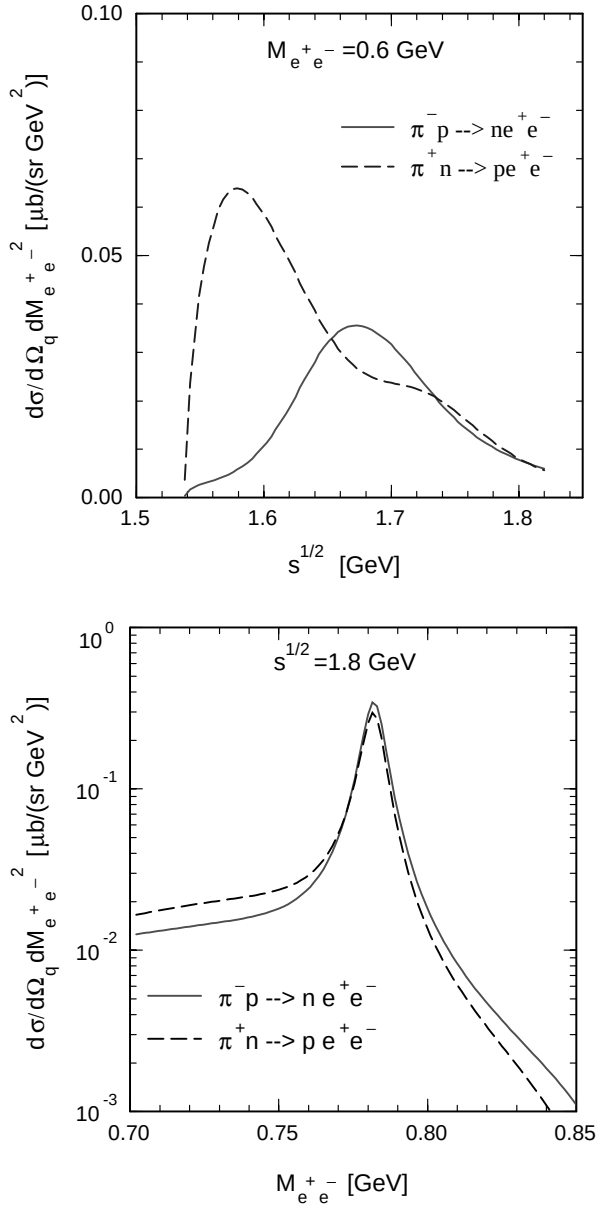

Fig. 11. Upper panel: the same as in the upper panel of fig. 8 but but with resonance parameters listed in table 2. Lower panel: the same as in the lower panel in fig. 3 but with resonance parameters listed in table 2.

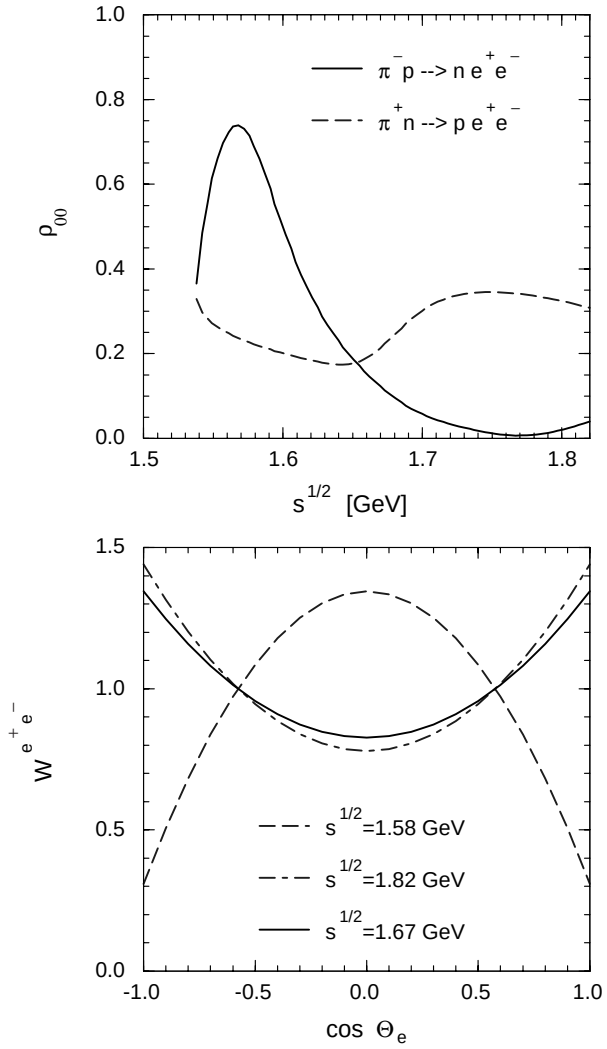

Fig. 12. The same as in fig. 9 but with resonance parameters listed in table 2.

tion $F(M)$ reads

$$F(M) = \mathrm{Sp}\left((\not{p}' + M_N)\mathcal{G}^{\mu,\kappa}\, \Pi_{\kappa,\kappa'}\, \mathcal{G}^{\nu,\kappa'}\right) \times \left(-g_{\mu\nu} + \frac{q_\mu g_\nu}{M^2}\right), \quad (18)$$

where $\mathcal{G}^{\mu,\kappa}$ ($\kappa = 0, \alpha, \alpha\beta$) according to eqs. (8),(9) is taken from eqs. (A.3)-(A.13) and

$$\Pi_{\kappa,\kappa'} = \sum_r \mathcal{U}^r_\kappa \bar{\mathcal{U}}^r_{\kappa'}\,, \quad (19)$$

with $\mathcal{U}$ from eq. (B.19). The corresponding branching ratios and $g^{\rm fit}_{\rho N B^*}$ are shown in table 2, where the phases are taken the same as predicted by quark model [18] shown in table 1. One can see that some of the couplings in table 2 are smaller than the corresponding values in table 1 (cf. $P_{11}(1440)$, $D_{13}(1520)$, $S_{11}(1535)$, $S_{11}(1650)$, $D_{13}(1700)$, $D_{15}(1675)$, $F_{15}(1680)$), while for other resonances they are greater (cf. $P_{33}(1600)$, $S_{31}(1620)$, $D_{33}(1700)$, $P_{13}(1720)$). It should be emphasized that a calculation with $g^{\rm fit}_{\rho N B^*}$ is not fully self-consistent because one cannot fix the coupling $g_\omega N N^*$ by this method, rather for them we use the prediction of the quark model [18] as listed in table 1. Nevertheless, for methodical purposes and to elucidate the sensitivity of our results, we perform such a calculation and present the results.

In fig. 10 (upper panel) we show the individual contributions of resonances for the ρ channel of the reaction $\pi^+ n \to p e^+ e^-$ as a function of $s^{1/2}$. The resonances $S_{11}(1535)$ and, somewhat less important, $P_{11}(1440)$ dominate at low energy, while $P_{13}(1720)$ becomes stronger at higher energies; in between $S_{11}(1650)$ is important. The total contribution of the ρ-meson with this new parameter

set is smaller. The differential cross-sections are shown in fig. 10 (lower panel). The absolute value of the total cross-section is smaller than that shown in the upper panel of fig. 7. But qualitatively their behavior is similar for both parameter sets.

In fig. 11 we show the differential cross-section of dielectron production for the reactions $\pi^- p \to n e^+ e^-$ and $\pi^+ n \to p e^+ e^-$ as a function of $s^{1/2}$ at $M = 0.6$ GeV (upper panel) and as a function of M at $s^{1/2} = 1.8$ GeV (lower panel). The isospin effect is greater at low energy and low invariant mass, as shown in the upper panel.

In fig. 12 we show the energy dependence of the spin density matrix element ρ_{00} (upper panel) and electron angular distribution (lower panel) as in fig. 9. One can see a strong difference of ρ_{00} for the two reactions and a deviation from the results shown in fig. 9: a strong increase at low energy for the $\pi^+ n$ reaction, because of a sizable contribution of the $P_{11}(1440)$ resonance, and relatively small value of ρ_{00} at higher energy, because of the dominance of the $P_{13}(1720)$ resonance. Also the angular distributions change considerably for this new parameter set. This sensitivity clearly demonstrates the need of experimental data for constraining the parameter space.

4 Summary

In summary we have performed a combined analysis of the dielectron invariant-mass distributions for the exclusive reactions $\pi^- p \to n e^+ e^-$ and $\pi^+ n \to p e^+ e^-$ near the ω threshold. The differential cross-sections for the two reactions are different because of different ρ^0-ω interferences. The calculation is based on a resonance model with s and u channels, where the $\omega(\rho)NB^*$ couplings as well as the phases of the πNB^* couplings are either taken from the recent work [18] or, at least partially, are determined from resonance decays. The found isospin effect is sensitive to the resonance coupling parameters and therefore, may be used as a powerful tool for the study of the resonance dynamics in dielectron production processes.

We have shown that our predictions can be experimentally tested by measuring the angular distribution of decay particles in reactions of the type $\pi N \to NV \to N e^+ e^-$ which are accessible with the pion beam at the HADES spectrometer at GSI/Darmstadt [8]. (Notice that for the inverse reactions with real photons a sizeable isospin effect is found, see [25].) We propose for the first time a systematic study of the isoscalar part of the electromagnetic current by using a combined analysis of dielecton production in $\pi^+ n$ and $\pi^- p$ reactions. To this end it would be desirable to have at our disposal the ratio or the difference of the $\pi^+ n$ and $\pi^- p$ cross-sections (which might be deduced, *e.g.*, from the reactions $\pi^+ d$ and $\pi^- d$) as a function of both the invariant dilepton mass in the interval $M = 0.6 \cdots 0.8$ GeV and the energy in the interval $s^{1/2} = s^{1/2}_{\rm threshold} \cdots 1.9$ GeV. This quantity is most sensible for a study of the ρ-ω interference.

Finally, it should be stressed that the present investigation is completely based on the resonance model and therefore, is valid near threshold. At higher energy one has to include other mechanisms like meson exchange t channel amplitudes. Unfortunately, in this case one has to make some assumptions on the relative phase between t and s, u channels, which is hitherto unknown. However, we expect that the presented isospin effect will persist in this case too.

We gratefully acknowledge fruitful discussions with H.W. Barz, R. Dressler, S.B. Gerasimov, J. Ritman, and Gy. Wolf. In particular, B. Friman is thanked for a critical reading of the manuscript. One of the authors (A.I.T.) thanks for the warm hospitality of the nuclear theory group in the Research Center Rossendorf. This work is supported by BMBF grant 06DR921 and Heisenberg-Landau program.

Appendix A. Effective Lagrangians

The effective Lagrangians for ω production within the framework of the Riska-Brown model [18] are listed in ref. [15]. Therefore, here we focus on ρ production (the effective interaction Lagrangians needed for ω production follow from the formulas below by the substitution $\boldsymbol{\rho} \to \omega$ and omitting corresponding isospin factors, and skipping the Δ and Δ^* contributions). For completeness we also include interactions with pions. With the notation of subsect. 2.1, the relevant expressions read

$$\mathcal{L}^{N_{\frac{1}{2}^+}(940)N}_{\pi,\rho NN} = \bar\psi_N \Bigg[- \frac{f_{\pi NN}}{m_\pi} \gamma_5 \gamma_\mu \, \partial^\mu \boldsymbol{\pi} \cdot \boldsymbol{\tau} - g_{\rho NN} \left(\gamma_\mu - \frac{\kappa_{\rho NN}}{2M_N} \sigma_{\mu\nu} \partial^\nu \right) \boldsymbol{\rho}^\mu \cdot \boldsymbol{\tau} \Bigg] \psi_N, \tag{A.1}$$

$$\mathcal{L}^{\Delta_{\frac{3}{2}^+}(1232)P_{33}}_{\pi,\rho N\Delta} = \bar\psi_N \Bigg[i \frac{f^{1232}_{\pi N\Delta}}{m_\pi} \, \partial^\alpha \boldsymbol{\pi} \cdot \boldsymbol{\chi} - \frac{g^{1232}_{\rho NN^*}}{M_\Delta + M_N} \gamma_5 \times \left(\gamma_\mu \partial^\alpha - g^\alpha_\mu \, \partial\!\!\!/ \right) \boldsymbol{\rho}^\mu \cdot \boldsymbol{\chi} \Bigg] \psi_{\Delta\alpha} + \text{h.c.}, \tag{A.2}$$

$$\mathcal{L}^{N_{\frac{1}{2}^+}(1440)P_{11}}_{\pi,\rho NN^*} = \bar\psi_N \Bigg[- \frac{f^{1440}_{\pi NN^*}}{m_\pi} \gamma_5 \gamma_\mu \, \partial^\mu \boldsymbol{\pi} \cdot \boldsymbol{\tau} - g^{1440}_{\rho NN^*} \times \left(\gamma_\mu + \partial_\mu \, \partial\!\!\!/ m_\rho^{-2} - \frac{\kappa_{\rho NN^*}}{M_{N^*} - M_N} \sigma_{\mu\nu} \partial^\nu \right) \boldsymbol{\rho}^\mu \cdot \boldsymbol{\tau} \Bigg] \times \psi_{N^*} + \text{h.c.}, \tag{A.3}$$

$$\mathcal{L}^{N_{\frac{3}{2}^-}(1520)D_{13}}_{\pi,\rho NN^*} = \bar\psi_N \Bigg[i \frac{f^{1520}_{\pi NN^*}}{m_\pi} \gamma_5 \, \partial^\alpha \boldsymbol{\pi} \cdot \boldsymbol{\tau} + \frac{g^{1520}_{\rho NN^*}}{m_\rho^2} \sigma_{\mu\nu} \partial^\nu \partial^\alpha \boldsymbol{\rho}^\mu \cdot \boldsymbol{\tau} \Bigg] \psi_{N^*\alpha} + \text{h.c.}, \tag{A.4}$$

$$\mathcal{L}^{N_{\frac{1}{2}^-}(1535)S_{11}}_{\pi,\rho NN^*} = \bar\psi_N \Bigg[- \frac{f^{1535}_{\pi NN^*}}{m_\pi} \gamma_\mu \, \partial^\mu \boldsymbol{\pi} \cdot \boldsymbol{\tau} - g^{1535}_{\rho NN^*} \gamma_5$$

$$\times(\gamma_\mu + \partial_\mu \not{\partial} m_\rho^{-2})\boldsymbol{\rho}^\mu \cdot \boldsymbol{\tau}\Big] \psi_{N^*} + \text{h.c.}, \quad (A.5)$$

$$\mathcal{L}^{\Delta_{\frac{3}{2}^+}(1600)P_{33}}_{\pi,\rho N\Delta} = \bar\psi_N \Big[i\frac{f^{1600}_{\pi N\Delta^*}}{m_\pi}\,\partial^\alpha \boldsymbol{\pi}\cdot\boldsymbol{\chi} - \frac{g^{1600}_{\rho N\Delta^*}}{M_{\Delta^*}+M_N}\gamma_5$$
$$\times\left(\gamma_\mu\partial^\alpha - g^\alpha_\mu\,\not{\partial}\right)\boldsymbol{\rho}^\mu\cdot\boldsymbol{\chi}\Big]\psi_{\Delta\alpha} + \text{h.c.}, \quad (A.6)$$

$$\mathcal{L}^{\Delta_{\frac{1}{2}^-}(1620)S_{31}}_{\pi,\rho N\Delta^*} = \bar\psi_N \Big[-\frac{f^{1620}_{\pi N\Delta^*}}{m_\pi}\gamma_\mu\,\partial^\mu \boldsymbol{\pi}\cdot\boldsymbol{\chi}$$
$$-g^{1620}_{\rho N\Delta^*}\gamma_5(\gamma_\mu + \partial_\mu\not{\partial} m_\rho^{-2})\boldsymbol{\rho}^\mu\cdot\boldsymbol{\chi}\Big]\psi_\Delta + \text{h.c.}, \quad (A.7)$$

$$\mathcal{L}^{N_{\frac{1}{2}^-}(1650)S_{11}}_{\pi,\rho NN^*} = \bar\psi_N \Big[-\frac{f^{1650}_{\pi NN^*}}{m_\pi}\gamma_\mu\,\partial^\mu \boldsymbol{\pi}\cdot\boldsymbol{\tau} - g^{1650}_{\rho NN^*}\gamma_5$$
$$\times(\gamma_\mu + \partial_\mu\not{\partial} m_\rho^{-2})\boldsymbol{\rho}^\mu\cdot\boldsymbol{\tau}\Big]\psi_{N^*} + \text{h.c.}, \quad (A.8)$$

$$\mathcal{L}^{N_{\frac{5}{2}^-}(1675)D_{15}}_{\pi,\rho NN^*} = \bar\psi_N \Big[-\frac{f^{1675}_{\pi NN^*}}{m_\pi^2}\,\partial^\alpha\partial^\beta \boldsymbol{\pi}\cdot\boldsymbol{\tau}$$
$$+\frac{g^{1675}_{\rho NN^*}}{m_\rho^2}\epsilon^{\alpha\gamma\mu\nu}\,\gamma_\nu\,\partial_\gamma\partial^\beta\boldsymbol{\rho}^\mu\cdot\boldsymbol{\tau}\Big]\psi_{N^*\alpha\beta} + \text{h.c.}, \quad (A.9)$$

$$\mathcal{L}^{N_{\frac{5}{2}^+}(1680)F_{15}}_{\pi,\rho NN^*} = \bar\psi_N \Big[-i\frac{f^{1680}_{\pi NN^*}}{m_\pi^2}\gamma_5\partial^\alpha\partial^\beta \boldsymbol{\pi}\cdot\boldsymbol{\tau} + \frac{g^{1680}_{\rho NN^*}}{m_\rho^2}$$
$$\times(\gamma_\mu + \partial_\mu\not{\partial} m_\rho^{-2})\partial^\alpha\partial^\beta\boldsymbol{\rho}^\mu\cdot\boldsymbol{\tau}\Big]\psi_{N^*\alpha\beta} + \text{h.c.}, \quad (A.10)$$

$$\mathcal{L}^{\Delta_{\frac{3}{2}^-}(1700)D_{33}}_{\pi,\rho N\Delta^*} = \bar\psi_N \Big[i\frac{f^{1700}_{\pi N\Delta^*}}{m_\pi}\gamma_5\partial^\alpha \boldsymbol{\pi}\cdot\boldsymbol{\chi}$$
$$+\frac{g^{1700}_{\rho N\Delta^*}}{m_\rho^2}\sigma_{\mu\nu}\partial^\nu\partial^\alpha\boldsymbol{\rho}^\mu\cdot\boldsymbol{\chi}\Big]\psi_{\Delta\alpha} + \text{h.c.}, \quad (A.11)$$

$$\mathcal{L}^{N_{\frac{3}{2}^-}(1700)D_{13}}_{\pi,\rho NN^*} = \bar\psi_N \Big[i\frac{f^{1700}_{\pi NN^*}}{m_\pi}\gamma_5\partial^\alpha \boldsymbol{\pi}\cdot\boldsymbol{\tau}$$
$$+\frac{g^{1700}_{\rho NN^*}}{m_\rho^2}\sigma_{\mu\nu}\partial^\nu\partial^\alpha\boldsymbol{\rho}^\mu\cdot\boldsymbol{\tau}\Big]\psi_{N^*\alpha} + \text{h.c.}, \quad (A.12)$$

$$\mathcal{L}^{N_{\frac{3}{2}^+}(1720)P_{13}}_{\pi,\rho NN^*} = \bar\psi_N \Big[i\frac{f^{1720}_{\pi NN^*}}{m_\pi}\partial^\alpha \boldsymbol{\pi}\cdot\boldsymbol{\tau} - \frac{g^{1720}_{\rho NN^*}}{M_{N^*}+M_N}\gamma_5$$
$$\times\left(\gamma_\mu\partial^\alpha - g^\alpha_\mu\,\not{\partial}\right)\boldsymbol{\rho}^\mu\cdot\boldsymbol{\tau}\Big]\psi_{N^*\alpha} + \text{h.c.}\,. \quad (A.13)$$

We use the convention of Bjorken and Drell [26] in definitions of γ matrices and the spin matrix $\sigma_{\mu\nu}$. The expressions, eqs. (A.1)-(A.13), are based on [18].

Appendix B. Invariant amplitudes

Here we list the explicit expressions for the amplitudes $\mathcal{A}^\mu(N^*) \equiv \mathcal{A}^{(\rho)\mu}(N^*) = \mathcal{A}^{(\rho)\mu}_s(N^*) - \mathcal{A}^{(\rho)\mu}_u(N^*)$ (expressions for ω production follow from them in a straightforward way) and $\mathcal{A}^\mu(\Delta^*) \equiv \mathcal{A}^{(\rho)\mu}(\Delta^*) = \mathcal{A}^{(\rho)\mu}_s(\Delta^*) + \mathcal{A}^{(\rho)\mu}_u(\Delta^*)$ in eq. (12),

$$\mathcal{A}_\mu(N^{940}) =$$
$$-i\frac{\Gamma^{(\rho)}_\mu(-q)\Lambda(p_L,M_{N^*})\gamma_5\,\not{k}F_N(s)}{s-m_N^2}$$
$$+i\frac{\gamma_5\,\not{k}\Lambda(p_R,M_{N^*})\Gamma^{(\rho)}_\mu(-q)F_N(u)}{u-m_N^2}, \quad (B.1)$$

$$\mathcal{A}_\mu(\Delta^{1232}) =$$
$$-i\frac{\gamma_5(q^\alpha\gamma_\mu - g^\alpha_\mu\,\not{q})\Lambda_{\alpha\beta}(p_L,M_\Delta)k^\beta F_\Delta(s)}{(M_\Delta+M_N)(s-M_\Delta^2+i\Gamma_\Delta M_\Delta)}$$
$$-i\frac{k^\beta\Lambda_{\beta\alpha}(p_R,M_\Delta)\gamma_5\,(q^\alpha\gamma_\mu - g^\alpha_\mu\,\not{q})\,F_\Delta(u)}{(M_\Delta+M_N)(u-M_\Delta^2+i\Gamma_\Delta M_\Delta)}, \quad (B.2)$$

$$\mathcal{A}_\mu(N^{1440}) =$$
$$-i\frac{(\gamma_\mu + \frac{\kappa_{\rho NN^*}}{M_{N^*}-M_N}q_\mu)\Lambda(p_L,M_{N^*})\gamma_5\,\not{k}F_{N^*}(s)}{s-M_{N^*}^2+i\Gamma_{N^*}M_{N^*}}$$
$$+i\frac{\gamma_5\,\not{k}\Lambda(p_R,M_{N^*})(\gamma_\mu + \frac{\kappa_{\rho NN^*}}{M_{N^*}-M_N}q_\mu)F_{N^*}(u)}{u-M_{N^*}^2+i\Gamma_{N^*}M_{N^*}}, \quad (B.3)$$

$$\mathcal{A}_\mu(N^{1520}) =$$
$$-\frac{\sigma_{\mu\nu}q^\nu q^\alpha\Lambda_{\alpha\beta}(p_L,M_{N^*})\gamma_5 k^\beta F_{N^*}(s)}{m_\rho^2(s-M_{N^*}^2+i\Gamma_{N^*}M_{N^*})}$$
$$+\frac{\gamma_5 k^\alpha\Lambda_{\alpha\beta}(p_R,M_{N^*})\sigma_{\mu\nu}\,q^\nu q^\beta F_{N^*}(u)}{m_\rho^2(u-M_{N^*}^2+i\Gamma_{N^*}M_{N^*})}, \quad (B.4)$$

$$\mathcal{A}_\mu(N^{1535}) =$$
$$-i\frac{\gamma_5\gamma_\mu\Lambda(p_L,M_{N^*})\,\not{k}F_{N^*}(s)}{s-M_{N^*}^2+i\Gamma_{N^*}M_{N^*}}$$
$$+i\frac{\not{k}\Lambda(p_R,M_{N^*})\gamma_5\gamma_\mu F_{N^*}(u)}{u-M_{N^*}^2+i\Gamma_{N^*}M_{N^*}}, \quad (B.5)$$

$$\mathcal{A}_\mu(\Delta^{1600}) =$$
$$-i\frac{\gamma_5\,(q^\alpha\gamma_\mu - g^\alpha_\mu\,\not{q})\,\Lambda_{\alpha\beta}(p_L,M_{\Delta^*})k^\beta F_{\Delta^*}(s)}{(M_{\Delta^*}+M_N)(s-M_{\Delta^*}^2+i\Gamma_{\Delta^*}M_{\Delta^*})}$$
$$-i\frac{k^\beta\Lambda_{\beta\alpha}(p_R,M_{\Delta^*})\gamma_5\,(q^\alpha\gamma_\mu - g^\alpha_\mu\,\not{q})\,F_{\Delta^*}(u)}{(M_{\Delta^*}+M_N)(u-M_{\Delta^*}^2+i\Gamma_{\Delta^*}M_{\Delta^*})}, \quad (B.6)$$

$$\mathcal{A}_\mu(\Delta^{1620}) =$$
$$-i\frac{\gamma_5\gamma_\mu\Lambda(p_L,M_{\Delta^*})\,\not{k}F_{\Delta^*}(s)}{s-M_{\Delta^*}^2+i\Gamma_{\Delta^*}M_{N\Delta^*}}$$
$$-i\frac{\not{k}\Lambda(p_R,M_{\Delta^*})\gamma_5\gamma_\mu F^*_\Delta(u)}{u-M_{\Delta^*}^2+i\Gamma_{\Delta^*}M_{\Delta^*}}, \quad (B.7)$$

$$\mathcal{A}_\mu(N^{1650}) =$$
$$-i\frac{\gamma_5\gamma_\mu \Lambda(p_L, M_{N^*})\, \not{k} F_{N^*}(s)}{s - M_{N^*}^2 + i\Gamma_{N^*}M_{N^*}}$$
$$+i\frac{\not{k}\Lambda(p_R, M_{N^*})\gamma_5\gamma_\mu F_{N^*}(u)}{u - M_{N^*}^2 + i\Gamma_{N^*}M_{N^*}}, \quad \text{(B.8)}$$

$$\mathcal{A}_\mu(N^{1675}) =$$
$$-\frac{\epsilon^\alpha_{\tau\mu\nu}q^\tau q^\beta k^\gamma k^\delta}{m_\pi m_\rho^2}\left(\frac{\gamma^\nu \Lambda_{\alpha\beta,\gamma\delta}(p_L, M_{N^*})F_{N^*}(s)}{s - M_{N^*}^2 + i\Gamma_{N^*}M_{N^*}}\right.$$
$$\left. - \frac{\Lambda_{\gamma\delta,\alpha\beta}(p_R, M_{N^*})\gamma^\nu F_{N^*}(u)}{u - M_{N^*}^2 + i\Gamma_{N^*}M_{N^*}}\right), \quad \text{(B.9)}$$

$$\mathcal{A}_\mu(N^{1680}) =$$
$$-i\frac{q^\alpha q^\beta k^\gamma k^\delta}{m_\pi m_\rho^2}\left(\frac{\gamma_\mu \Lambda_{\alpha\beta,\gamma\delta}(p_L, M_{N^*})\,\gamma_5 F_{N^*}(s)}{s - M_{N^*}^2 + i\Gamma_{N^*}M_{N^*}}\right.$$
$$\left. - \frac{\gamma_5\Lambda_{\gamma\delta,\alpha\beta}(p_R, M_{N^*})\,F_{N^*}(u)}{u - M_{N^*}^2 + i\Gamma_{N^*}M_{N^*}}\right),$$

$$\mathcal{A}_\mu(\Delta^{1700}) =$$
$$-\frac{\sigma_{\mu\nu}q^\nu q^\alpha \Lambda_{\alpha\beta}(p_L, M_{\Delta^*})\,\gamma_5 k^\beta F_{\Delta^*}(s)}{m_\rho^2(s - M_{\Delta^*}^2 + i\Gamma_{\Delta^*}M_{\Delta^*})}$$
$$-\frac{\gamma_5 k^\alpha \Lambda_{\alpha\beta}(p_R, M_{\Delta^*})\sigma_{\mu\nu}q^\nu q^\beta F_{\Delta^*}(u)}{m_\rho^2(u - M_{\Delta^*}^2 + i\Gamma_{\Delta^*}M_{\Delta^*})}, \quad \text{(B.10)}$$

$$\mathcal{A}_\mu(N^{1700}) =$$
$$-\frac{\sigma_{\mu\nu}q^\nu q^\alpha \Lambda_{\alpha\beta}(p_L, M_{N^*})\,\gamma_5 k^\beta F_{N^*}(s)}{m_\rho^2(s - M_{N^*}^2 + i\Gamma_{N^*}M_{N^*})}$$
$$+\frac{\gamma_5 k^\alpha \Lambda_{\alpha\beta}(p_R, M_{N^*})\sigma_{\mu\nu}q^\nu q^\beta F_{N^*}(u)}{m_\rho^2(u - M_{N^*}^2 + i\Gamma_{N^*}M_{N^*})}, \quad \text{(B.11)}$$

$$\mathcal{A}_\mu(N^{1720}) =$$
$$-i\frac{\gamma_5(q^\alpha\gamma_\mu - g_\mu^\alpha \not{q})\,\Lambda_{\alpha\beta}(p_L, M_{N^*})k^\beta F_{N^*}(s)}{(M_{N^*} + M_N)(s - M_{N^*}^2 + i\Gamma_{N^*}M_{N^*})}$$
$$+i\frac{k^\beta \Lambda_{\beta\alpha}(p_R, M_{N^*})\gamma_5(q^\alpha\gamma_\mu - g_\mu^\alpha \not{q})F_{N^*}(u)}{(M_{N^*} + M_N)(u - M_{N^*}^2 + i\Gamma_{N^*}M_{N^*})}, \quad \text{(B.12)}$$

with $p_L = p + k$, $p_R = p - q$ and

$$\Gamma^{(\rho)}_\alpha(k_{(\rho)}) = \gamma_\alpha + i\frac{\kappa_{\rho NN}}{2M_N}\sigma_{\alpha\beta}\,k^\beta_{(\rho)}. \quad \text{(B.13)}$$

For completeness, we display also expressions for propagators and Rarita-Schwinger spinors. The resonance propagators in eqs. (B.1)-(B.12) are defined by the conventional method [27] assuming the validity of the spectral decomposition

$$\psi_{N^*}(x) = \int \frac{\mathrm{d}^3\mathbf{p}}{(2\pi)^3\sqrt{2E_p}} \times \left[a_{\mathbf{p},r}u^r_{N^*}(p)e^{-ipx} + b^+_{\mathbf{p},r}v^r_{N^*}(p)e^{+ipx}\right]. \quad \text{(B.14)}$$

The finite decay width Γ_{N^*} is introduced into the propagator denominators by substituting $M_{N^*} \to M_{N^*} - \frac{i}{2}\Gamma_{N^*}$.

Therefore, the operators $\Lambda_{\ldots}(p, M)$ are defined as

$$\Lambda(p, M) = \frac{1}{2}\sum_r\left(\left(1 + \frac{p_0}{E_0}\right)u^r(\mathbf{p}, E_0)\otimes\bar{u}^r(\mathbf{p}, E_0)\right.$$
$$\left. - \left(1 - \frac{p_0}{E_0}\right)v^r(-\mathbf{p}, E_0)\otimes\bar{v}^r(-\mathbf{p}, E_0)\right) = \not{p} + M, \quad \text{(B.15)}$$

$$\Lambda_{\alpha\beta}(p, M) = \frac{1}{2}\sum_r\left(\left(1 + \frac{p_0}{E_0}\right)\mathcal{U}^r_\alpha(\mathbf{p}, E_0)\otimes\bar{\mathcal{U}}^r_\beta(\mathbf{p}, E_0)\right.$$
$$\left. - \left(1 - \frac{p_0}{E_0}\right)\mathcal{V}^r_\alpha(-\mathbf{p}, E_0)\otimes\bar{\mathcal{V}}^r_\beta(-\mathbf{p}, E_0)\right), \quad \text{(B.16)}$$

$$\Lambda_{\alpha\beta,\gamma\delta}(p, M) = \frac{1}{2}\sum_r\left(\left(1 + \frac{p_0}{E_0}\right)\mathcal{U}^r_{\alpha\beta}(\mathbf{p}, E_0)\otimes\bar{\mathcal{U}}^r_{\gamma\delta}(\mathbf{p}, E_0)\right.$$
$$\left. - \left(1 - \frac{p_0}{E_0}\right)\mathcal{V}^r_{\alpha\beta}(-\mathbf{p}, E_0)\otimes\bar{\mathcal{V}}^r_{\gamma\delta}(-\mathbf{p}, E_0)\right), \quad \text{(B.17)}$$

where $E_0 = \sqrt{\mathbf{p}^2 + M^2}$, and the Rarita-Schwinger spinors read

$$\mathcal{U}^r_\alpha(p) = \sum_{\lambda,s}\left\langle 1\lambda\frac{1}{2}s\middle|\frac{3}{2}r\right\rangle\varepsilon^\lambda_\alpha(p)u^s(p), \quad \text{(B.18)}$$

$$\mathcal{U}^r_{\alpha\beta}(p) = \sum_{\lambda,\lambda' s,t}\left\langle 1\lambda\frac{1}{2}s\middle|\frac{3}{2}t\right\rangle \times\left\langle\frac{3}{2}t1\lambda'\middle|\frac{5}{2}r\right\rangle\varepsilon^\lambda_\alpha(p)\varepsilon^{\lambda'}_\beta(p)u^s(p). \quad \text{(B.19)}$$

The spinors v and $\mathcal{V}$ are related to u and $\mathcal{U}$ as $v(p) = i\gamma_2\,u^*(p)$ and $\mathcal{V}(p) = i\gamma_2\mathcal{U}^*(p)$, respectively. In our calculations we use energy-dependent total resonance decay widths Γ_{N^*}. However, taking into account that the effect of a finite width is quite different for s and u channels, because of the evident relation $|u| + M_{N^*}^2 \gg |s - M_{N^*}^2|$, we use $\Gamma_{N^*} = \Gamma^0_{N^*}$ for the u channels and

$$\Gamma_{N^*} = \Gamma^0_{N^*}\left[1 - B^\pi_{N^*} + B^\pi_{N^*}\left(\frac{\mathbf{k}}{\mathbf{k}_0}\right)^{2J}\right] \quad \text{(B.20)}$$

for the s channels, where $\Gamma^0_{N^*}$ is the total on-shell resonance decay width and $B^\pi_{N^*}$ stands for the branching ratio of the $N^* \to N\pi$ decay channel taken from [20]; $\mathbf{k}_0$ is the pion momentum at the resonance position, *i.e.* at $\sqrt{s} = M_{N^*}$, and the factor $(\mathbf{k}/\mathbf{k}_0)^{2J}$ comes from a direct calculation of the $N^* \to N\pi$ decay width using the effective Lagrangians of eqs. (A.3)-(A.13), where we keep the leading term proportional to $\mathbf{k}^{2J}$.

References

1. CERES collaboration (G. Agakishiev et al.), Phys. Rev. Lett. **75**, 1272 (1995).
2. W. Cassing, E.L. Bratkovskaya, Phys. Rep. **308**, 65 (1999).

3. R. Rapp, J. Wambach, Adv. Nucl. Phys. **25**, 1 (2000).
4. G.E. Brown, M. Rho, hep-ph/0103102.
5. M.A. Shifman, A.I. Vainstein, V.I. Zakharov, Nucl. Phys. B **147**, 385 (1979); T. Hatsuda, S.H. Lee, Phys. Rev. C **46**, R34 (1992); A.K. Dutt-Mazumder, R. Hofmann, M. Pospelov, Phys. Rev. C **63**, 015204 (2001).
6. F. Klingl, N. Kaiser, W. Weise, Nucl. Phys. A **624**, 527 (1997); Z. Phys. A **356**, 193 (1996); F. Klingl, W. Weise, Eur. Phys. J. A **4**, 225 (1999); F. Klingl, T. Waas, W. Weise, Nucl. Phys. A **650**, 299 (1999); M. Urban, M. Buballa, J. Wambach, Nucl. Phys. A **673**, 357 (2000) and references therein.
7. DLS collaboration (R.J. Porter et al.), Nucl. Phys. A **638**, 499 (1998).
8. HADES collaboration (J. Friese et al.), GSI report 97-1, (1997) p. 193; Prog. Part. Nucl. Phys. **42**, 235 (1999).
9. M. Effenberger, E.L. Bratkovskaya, W. Cassing, U. Mosel, Phys. Rev. C **60**, 027601 (1999).
10. B. Friman, H.J. Pirner, Nucl. Phys. A **617**, 496 (1997).
11. B. Friman, Acta Phys. Polon. B **29**, 3195 (1998) .
12. M. Lutz, G. Wolf, B. Friman, Nucl. Phys. A **661**, 526 (1999); B. Friman, M. Lutz, G. Wolf, nucl-th/0003012; M. Lutz, G. Wolf, B. Friman, work in preparation.
13. M. Soyeur, M. Lutz, B. Friman, nucl-th/0003013.
14. M. Post, S. Leupold, U. Mosel, Nucl. Phys. A **689**, 753 (2001); M. Post, U. Mosel, Nucl. Phys. A **688**, 808 (2001).
15. A.I. Titov, B. Kämpfer, B.L. Reznik, nucl-th/0102032.
16. G.I. Lykasov, W. Cassing, A. Sibirtsev, M.V. Rzyanin, Eur. Phys. J. A **6**, 71 (1999).
17. N.M. Kroll, T.D. Lee, B. Zumino, Phys. Rev. **157**, 1376 (67).
18. D.O. Riska, G.E. Brown, Nucl. Phys. A **679**, 577 (2001).
19. D.M. Manley, E.M. Saleski, Phys. Rev. D **45**, 4002 (1992).
20. Particle Data Group (C. Caso et al.), Eur. Phys. J. C **3**, 1 (1998).
21. T. Feuster, U. Mosel, Phys. Rev. C **58**, 457 (1998); **59**, 460 (1999).
22. A.I. Titov, B. Kämpfer, B.L. Reznik, Eur. Phys. J. A **7**, 543 (2000).
23. R. Machleidt, Adv. Nucl. Phys. **19**, 189 (1989).
24. Th.A. Rijken, V.G.J. Stoks, Y. Yamamoto, Phys. Rev. C **59**, 21 (1999).
25. S. Nozawa, B. Blankleider, T.S.H. Lee, Nucl. Phys. A **513**, 459 (1990).
26. J.D. Bjorken, S.D. Drell, *Relativistic Quantum Mechanics* (McGraw-Hill, 1964).
27. C. Itzykson, J.-B. Zuber, *Quantum Field Theory* (McGraw-Hill, Singapore, 1985).